Uncovering distinct progression patterns of tau deposition in progressive supranuclear palsy using [^{18}F]Florzolotau PET imaging and subtype/stage inference algorithm

Jimin Hong,[b,c,n] Jiaying Lu,[a,b,d,n] Fengtao Liu,[d,e,n] Min Wang,[f,g] Xinyi Li,[d,e] Christoph Clement,[b,c] Leonor Lopes,[b,c] Matthias Brendel,[h,k,l] Axel Rominger,[b] Tzu-Chen Yen,[i] Yihui Guan,[a,d] Mei Tian,[a,j,m] Jian Wang,[d,e,**] Chuantao Zuo,[a,d,j,*] and Kuangyu Shi,[b,g] the Progressive Supranuclear Palsy Neuroimage Initiative (PSPNI)

[a]Department of Nuclear Medicine & PET Center, Huashan Hospital, Fudan University, Shanghai, China
[b]Department of Nuclear Medicine, Inselspital, University of Bern, Bern, Switzerland
[c]Graduate School for Cellular and Biomedical Sciences, University of Bern, Switzerland
[d]National Center for Neurological Disorders & National Clinical Research Center for Aging and Medicine, State Key Laboratory of Medical Neurobiology, Huashan Hospital, Fudan University, Shanghai, China
[e]Department of Neurology, Huashan Hospital, Fudan University, Shanghai, China
[f]Institute of Biomedical Engineering, School of Life Science, Shanghai University, Shanghai, China
[g]Department of Informatics, Technical University of Munich, Munich, Germany
[h]Department of Nuclear Medicine, University of Munich, Munich, Germany
[i]APRINOIA Therapeutics Co., Ltd, Suzhou, China
[j]Human Phenome Institute, Fudan University, Shanghai, China
[k]German Center for Neurodegenerative Diseases (DZNE), Munich, Germany
[l]Munich Cluster for Systems Neurology (SyNergy), Munich, Germany
[m]International Human Phenome Institutes (Shanghai), Shanghai, China

eBioMedicine
2023;97: 104835
Published Online xxx
https://doi.org/10.1016/j.ebiom.2023.104835

Summary

Background Progressive supranuclear palsy (PSP) is a primary 4-repeat tauopathy with diverse clinical phenotypes. Previous *post-mortem* studies examined tau deposition sequences in PSP, but *in vivo* scrutiny is lacking.

Methods We conducted [^{18}F]Florzolotau tau positron emission tomography (PET) scans on 148 patients who were clinically diagnosed with PSP and 20 healthy controls. We employed the Subtype and Stage Inference (SuStaIn) algorithm to identify PSP subtype/stage and related tau patterns, comparing clinical features across subtypes and assessing PSP stage-clinical severity association. We also evaluated functional connectivity differences among subtypes through resting-state functional magnetic resonance imaging.

Findings We identified two distinct subtypes of PSP: Subtype1 and Subtype2. Subtype1 typically exhibits a sequential progression of the disease, starting from subcortical and gradually moving to cortical regions. Conversely, Subtype2 is characterized by an early, simultaneous onset in both regions. Interestingly, once the disease is initiated, Subtype1 tends to spread more rapidly within each region compared to Subtype2. Individuals categorized as Subtype2 are generally older and exhibit less severe dysfunctions in areas such as cognition, bulbar, limb motor, and general motor functions compared to those with Subtype1. Moreover, they have a more favorable prognosis in terms of limb motor function. We found significant correlations between several clinical variables and the identified PSP SuStaIn stages. Furthermore, Subtype2 displayed a remarkable reduction in functional connectivity compared to Subtype1.

Interpretation We present the evidence of distinct *in vivo* spatiotemporal tau trajectories in PSP. Our findings can contribute to precision medicine advancements for PSP.

Funding This work was supported by grants from the National Natural Science Foundation of China (number 82272039, 81971641, 82021002, and 92249302); Swiss National Science Foundation (number 188350); the STI2030-Major Project of China (number 2022ZD0211600); the Clinical Research Plan of Shanghai Hospital Development Center of China (number SHDC2020CR1038B); and the National Key R&D Program of China (number 2022YFC2009902, 2022YFC2009900), the China Scholarship Council (number 202006100181); the Deutsche

*Corresponding author. Department of Nuclear Medicine & PET Center, Huashan Hospital, Fudan University, Shanghai, China.
**Corresponding author. Department of Neurology, Huashan Hospital, Fudan University, Shanghai, China.
E-mail addresses: zuochuantao@fudan.edu.cn (C. Zuo), wangjian_hs@fudan.edu.cn (J. Wang).
[n]Equally contributed.

Forschungsgemeinschaft (DFG) under Germany's Excellence Strategy within the framework of the Munich Cluster for Systems Neurology (EXC 2145 SyNergy, ID 390857198).

Keywords: Progressive supranuclear palsy; [^{18}F]Florzolotau tau positron emission tomography imaging; Spatiotemporal trajectories; Machine learning

Research in context

Evidence before this study

Progressive supranuclear palsy (PSP) is a primary 4-repeat (4R) tauopathy that presents with a diverse range of clinical phenotypes. Previous postmortem studies have reported that tau pathology in PSP is heterogeneous. Recently, a new-generation radiotracer, [^{18}F]Florzolotau, has been developed, which has demonstrated the capability to capture the distribution patterns and regional vulnerability of tau pathology in living brains of PSP. Notably, the recent postmortem suggests that the tau patterns in various clinical phenotypes of PSP, including Richardson's syndrome (PSP-RS) and the variants of PSP (vPSP), are similar, although tau accumulation appears to be more prominent in PSP-RS than in vPSP. To date, there has been limited research on the phenotypic and temporal trajectory of tau deposition in PSP *in vivo*, and most studies focus on either modeling the temporal heterogeneity (i.e., stage) or on phenotypic heterogeneity (i.e., subtype) but not both simultaneously.

Added value of this study

In this study, an approach that combined [^{18}F]Florzolotau positron emission tomography (PET) imaging, which shows higher binding affinity to 4R tau compared to the first-generation tau tracers, with the unsupervised machine learning algorithm Subtype and Stage Inference (SuStaIn), was used to model the heterogeneous spatiotemporal patterns of tau deposition in PSP. This allowed us to profile and stratify the subtypes and stages of PSP, as well as the changes in the tau deposition and the related clinical features. By utilizing this technique to explore tau pathology in PSP *in vivo*, this study provided valuable insights into the underlying pathological and clinical heterogeneity of PSP.

Implications of all the available evidence

The findings of heterogeneous tau deposition in PSP have significant implications for the increasing number of new tau-targeting therapy trials and may facilitate the development of personalized treatment strategies for PSP patients.

Introduction

Progressive supranuclear palsy (PSP) is a primary 4-repeat (4R) tauopathy that involves the gradual deterioration of behavioral, language, and movement.[1] The cumulative evidence suggests that PSP is characterized by a sequence of neuropathological events that begins with an asymptomatic phase and progresses to a symptomatic phase,[2–4] during which specific vulnerable regions give rise to distinct clinical phenotypes.[5] The most prevalent subtype is Richardson's syndrome (PSP-RS), and other clinical variants of PSP (vPSP, each named after its predominant clinical feature) eventually develop some or all of the clinical presentation of PSP-RS.[6,7]

Over the past few decades, efforts have been made to identify tau progression patterns that may differentiate the various clinical phenotypes of PSP.[5,8,9] The postmortem study by Kovacs and colleagues revealed the six distinct stages of tau progression in PSP,[8] which correlated with antemortem clinical severity.[10] In another work, the authors suggested that the initiating site of tau pathology is consistent across the clinical PSP subtypes in the pallido-nigro-luysian axis and that total tau load as well as cell-type (neuronal versus glial) define specific vulnerability patterns for each subtype.[8]

Positron emission tomography (PET) imaging enables the *in vivo* measurement of tau accumulation in the brain.[11–14] However, the first-generation tau PET ligand, [^{18}F]Flortaucipir, has exhibited limited success in PSP studies, possibly due to its relatively low binding affinity to 4R-tau and non-negligible off-target binding.[8,13,14] Recently, new-generation tau tracers have been developed, demonstrating high binding affinity to both 3-repeat (3R) and 4R-tau. Amongst these, [^{18}F]Florzolotau (also known as [^{18}F]APN-1607 or [^{18}F]PM-PBB3[11]) has shown considerable promises for diagnosing, differentiating, and assessing disease severity in PSP patients[12] based on tau distribution patterns and regional vulnerability.[15] Current studies indicate that the tau distribution patterns of PSP-RS and vPSP are similar.[8,15,16] With the advancements made by [^{18}F]Florzolotau, it is now an opportune time to systemically investigate the heterogeneous spatiotemporal trajectories of tau in PSP. The unsupervised machine-learning algorithm, Subtype and Stage Inference (SuStaIn) algorithm, is expected to achieve breakthroughs in PSP stratification, by simultaneously modeling temporal heterogeneity (i.e., stage) and phenotypic heterogeneity (i.e., subtype) with cross-sectional data alone.[17–20] The previous trajectory studies

assumed that all individuals have a single phenotype with approximately the same progression. On the other hand, the differential diagnosis researches inherently require a *priori* that all subjects are at a common disease stage. SuStaIn overcomes this limitation by modeling both heterogeneities concurrently.

In this work, we elucidate the subtypes and stages of PSP by utilizing the SuStaIn algorithm on [^{18}F]Florzolotau PET scans from a large cohort that includes clinically diagnosed PSP patients. In particular, we examined the progression pattern of tau pathology in each subtype throughout its stages. We then compared the similarities and differences of clinical features among PSP subtypes and evaluated the relationship between PSP stages and clinical severity. Given that neuronal connectivity plays a crucial role in tau propagation, we investigated the functional connectivity (FC) differences between PSP subtypes using resting-state functional magnetic resonance imaging (rs-fMRI) which may provide insight into the underlying mechanisms driving the distinct tau pathways among subtypes.[21,22]

Methods

Ethics

The research approval was granted by the Institutional Review Board of the Huashan Hospital (identifiers: KY2019-284, KY2019-433, and KY2020-1160) and written informed consent in accordance with the Helsinki declaration was obtained from all participants and/or their legal proxy.

Participants

A total of 148 patients with PSP were enrolled from Progressive Supranuclear Palsy Neuroimage Initiative (PSPNI) between May 2019 and January 2022.[15] The clinical diagnosis of PSP was based on the latest Movement Disorder Society (MDS) clinical diagnosis criteria[1] by a panel of neurologists specializing in the field of movement disorders from Huashan Hospital, Fudan University (Shanghai, China). The details about inclusion and exclusion have been reported elsewhere.[15] 56.8% (n = 84) were clinically diagnosed with probable PSP-RS, and the other variants are referred to as PSP-non-RS (n = 64) in this work. The PSP-non-RS consisted of PSP-OM (n = 1), PSP-P (n = 28), PSP-PGF (n = 31), PSP-PI (n = 1), and PSP-SL (n = 3). A group of healthy controls (HCs, n = 20) was retrospectively enrolled from our previous project.[23] The general characteristics of all participants enrolled in this study are presented in Supplementary Table S1.

As of August 2022, 43 patients with PSP (29.1%) participated in at least one clinical follow-up after their baseline PET scan. The mean (standard deviation) interval between baseline and the first visit was 1.09 (0.26) year. Among them, 10 made a second clinical follow-up and the mean (standard deviation) interval between baseline and the second visit was 2.04 (0.28) year. The baseline characteristics of the longitudinal follow-up subset are summarized in Supplementary Table S2.

Clinical assessments

Clinical assessments of the patients with PSP were made after at least 12 h from the last dose of any anti-parkinsonian medication if used. The clinical severity of PSP patients were evaluated using PSP rating scale (PSPrs, total and stratified),[24] the ratings of MDS four core features [Ocular Motor Dysfunction (O), Postural Instability (P), Akinesia (A), Cognitive Dysfunction (C)],[1] part III of MDS Sponsored Revision of the Unified Parkinson's Disease Rating Scale (MDS UPDRS-III)[25] and the Hoehn and Yahr scale (H&Y). The stratified PSPrs consists of six items that measure each function: PSPrs-I (History), PSPrs-II (Mentation), PSPrs-III (Bulbar), PSPrs-IV (Ocular motor), PSPrs-V (Limb motor) and PSPrs-VI (Gait and midline). The Mini-Mental State Examination (MMSE) scores were measured to test global cognitive functioning, and the L-dopa equivalent daily dose (LEDD) scores were calculated. For HCs, the MMSE scores were collected, however, neither the clinical severity scores nor LEDD was measured. Therefore, in subsequent analyses that required the clinical severity scores of subjects that were HC, we linearly extrapolated the scores. For instance, the PSPrs score was set as 0 for HC, as the level of severity is higher in ascending order (0: lowest, and 100: highest).

Imaging acquisition and preprocessing

[^{18}F]Florzolotau PET scans (90–110 min after administration, static) were collected with the paired MRI for all subjects. The protocol parameters for both [^{18}F]Florzolotau PET and T1-MRI scans as well as the preprocessing of both scans can be found in the previous literature.[12,15] The individual PET images were spatially normalized to the Montreal Neurological Institute (MNI) space using the co-registered T1-MRI and smoothed (statistical parametric mapping, SPM12, www.fil.ion.ucl.ac.uk/spm). The standardized uptake value ratio (SUVr) was calculated by using the cerebellar gray matter as the reference region.

The protocol for rs-fMRI was consistent with previously reported article.[26] To mitigate the effects of diurnal fluctuations on our findings, all scans were consistently conducted during the morning hours. 5 patients with PSP and 3 HCs were excluded from rs-fMRI analysis due to their inability to accomplish the scanning or poor image quality. An experienced in-house neuroradiologist, Dr. Chuantao Zuo, conducted a comprehensive visual evaluation of additional sequences (T2 FLAIR, SWI, CT). The aim was to confirm that all potential participants were devoid of any indicators of intracranial hemosiderin/ferritin, brain tumors, cerebrovascular lesions, or calcification. rs-fMRI images were preprocessed in accordance with the previously reported

steps[27] (Data Processing Assistant for Resting-State fMRI (http://www.rfmri.org/DPARSF)), spatially normalized, and smoothed.[12,15]

SuStaIn model

SuStaIn is a probabilistic unsupervised machine-learning algorithm that infers both temporal and phenotypical heterogeneity (i.e., stage and subtype) from cross-sectional data.[17,19] It is a mixture of linear z-score model that is based on event-based model (EBM).[28,29] Unlike previous EBM where an event accounts for an instantaneous shift from a normal to an abnormal level, SuStaIn reformulates the event as a continuous linear accumulation of a biomarker that is represented as a set of z-scores.[17,30] SuStaIn is thereafter fitted in an iterative manner that simultaneously optimizes subtype membership, subtype trajectory and the posterior distribution of both. The model is first fitted with the single subtype and continues to be fitted with the predefined maximum number of subtypes hierarchically. The model is optimized using expectation maximization (EM) procedure, alternating between updating the sequence for each subtype and fraction of subjects assigned to a particular subtype. The detailed mathematical formalization of SuStaIn was published previously.[17] As SuStaIn is an unsupervised learning algorithm, there has been little consensus on how to divide data and validate the model. For this work, we randomly divided the data into two subgroups including 140 and 28 [^{18}F]Florzolotau PET scans and referred to as discovery and test set respectively (5:1). Both sets held the same ratio of PSP and HC. We did this in order to corroborate the subtype/stage findings from two independent datasets. In addition, we used 10-fold cross-validation in discovery data set to evaluate the optimal number of subtypes. The subtype/stage results given from each discovery, test and cross-validation set were compared to assess the consistency of our findings in subtype progression pattern. We summarized our findings made from the discovery set in the results section, unless specified otherwise.

SuStaIn input

SuStaIn model requires a collection of input that includes z-scores in each region of interests (ROIs), z-score cut-offs for each ROI, maximum z-score for each ROI, maximum number of subtypes, number of starting points for random subtype-cluster assignments and number of Markov Chain Monte Carlo (MCMC) sampling to provide the model uncertainty.[17,19] The study design is comprehensively illustrated in Fig. 1.

We selected 14 ROIs that encompasses the previously identified range of tau aggregation in PSP[8]: 10 subcortical regions [thalamus (TH), locus coeruleus (LC), raphe nuclei (Ra), dentate nucleus (DE), cerebellum white matter (CEWM), putamen (PU), substantia nigra (SN), globus pallidus (GP), subthalamic nucleus (STN), and red nucleus (RN)] and 4 cortical regions [frontal cortex (FR), parietal cortex (PA), occipital cortex (OC), temporal cortex (TE)]. All ROIs were extracted from public atlases according to the method of the previous literature.[15] Subsequently, z-scores for each ROI were computed using the mean and standard deviation determined by the SUVr distribution of HCs, after adjusting for age and sex. Given the relatively wide distribution of z-score (Supplementary Figure S1), we grouped 14 ROIs into 4 bundles based on their distribution and assigned each bundle to the subset of z-score cut-offs that contain the array of 1,3,5,8, and 13 (Supplementary Table S3). The maximum z-score achieved at the progression's final stage was set at 5, 7, 10, or 15, depending on whether the last cut-off was 3, 5, 8, or 13.

The maximum number of subtypes was set as 5. To determine the optimal number of subtypes, we assessed cross-validation information criteria (CVIC) and the histogram of model log-likelihood of each subtype, and compared the positional variance diagrams obtained from discovery, test, and cross-validation set. For the cross-validation set, the positional variance diagram is derived by averaging across folds. In this study, we set 25 starting points for random subtype-cluster assignment, and 100,000 MCMC iterations for estimating model uncertainty.

SuStaIn output

SuStaIn generates the most probable tau progression pattern for each subtype and estimates the uncertainty in the ordering of the given sequence. The positional variation diagram of this sequence is visualized using different colors which indicates the cumulative probability that each ROI has reached the z-cutoffs. The cumulative probability of each ROI going from z-score 0 to z-score 1-sigma were coated in the range of white and red. Similarly, magenta, blue, cyan, and green were used to mark z-score of 3,5,8, and 13-sigma, respectively. SuStaIn also provides the estimated probability of subtype and stage in individual-level. Subjects classified as stage 0 by SuStaIn were subsequently excluded from any subtype and collectively designated as subtype0, which represents the subtype devoid of any tau abnormality. The average z-values of individuals within each subtype along the progression stages were illustrated using BrainNet Viewer.[31] SuStaIn resulted in 43 stages in total, and we averaged the subjects that are in stage 1–8, in 9–16, in 17–24, in 25–32 and 33–41 for the figure.

Functional connectivity analysis

We carried out region-to-region FC analysis to find the underlying mechanism of distinct tau trajectories between subtypes. Assuming that the neuronal interaction between the brain regions occurs during the resting condition, FC is calculated by deriving the temporal

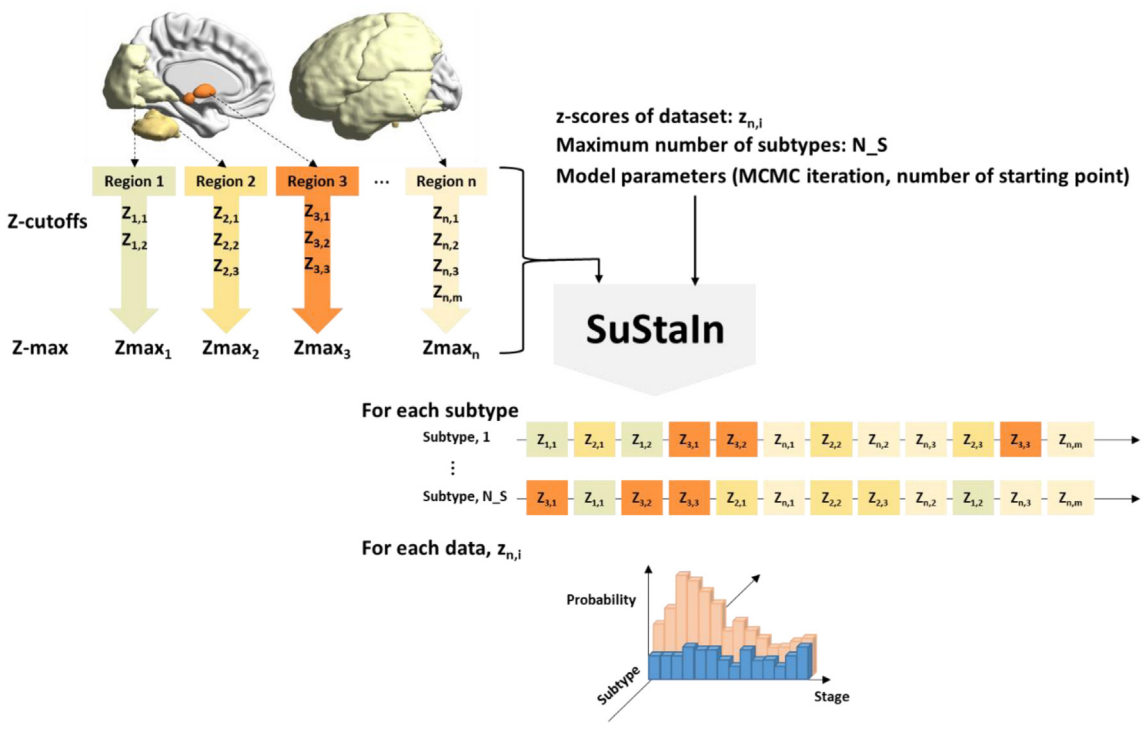

***Fig. 1:* Study design using Subtype and Staging Inference (SuStaIn)**. SuStaIn requires z-scores of dataset ($z_{n,j}$), maximum number of subtypes (N_S), z-score cutoffs ($Z_{n,m}$), maximum Z-score ($Zmax_n$) for the number of subjects (i), the number of regions (n), and the number of cut-offs (m). The model parameters such as the number of Markov Chain Monte Carlo (MCMC) iteration and the number of starting points for random subtype-cluster assignments is also required as an input. SuStaIn estimates not only the temporal progression of subtypes but also the probability of each individual being assigned to a particular subtype and stage.

correlation of blood-oxygen-level dependent (BOLD) time points between the pairs of brain regions using rs-fMRI scans. For each subject, FC between 14 ROIs, equivalent to the ROIs for SuStaIn analysis, was assessed by calculating partial correlations between time series for each pair of ROIs, yielding a 14 x 14 FC matrix. Covariates such as age, sex, education year, clinical diagnosis, LEDD, and SuStaIn stage were statistically adjusted. Correlation values were subsequently converted to Z-scores using Fisher r-to-z transformation and auto-correlations were set to zero. Group-average FC matrices were computed for each resulting PSP subtype. Lastly, the Z-statistic was employed to compare the Z-value maps and determine the significance of the between-subtype differences in correlations. A voxel threshold of $|Z| > 1.96$ (corresponding $p < 0.05$) was considered significant.

Statistical analysis

The clinical presentations of the identified subtypes were statistically compared with those of subtype0, as well as with each other. These included age, sex, education year, MMSE, clinical diagnosis (HC/PSP), clinical phenotypes of PSP (PSP-RS/PSP-non-RS), disease duration, LEDD, total and six stratified domains of the PSPrs, four core clinical features of PSP suggested by MDS, MDS UPDRS-III, and H&Y scale. The categorical data such as clinical diagnosis and clinical phenotypes were converted to numerical values for the statistical analysis.

For the comparison with subtype0, a generalized linear model (GLM) was fitted with each clinical feature as a dependent variable and with a dummy-coded subtype as an independent variable where subtype0 was coded as the reference subtype. Age, sex, education year, clinical diagnosis, and LEDD were entered as covariates, and each variable was excluded for its turn when it was used as a dependent variable. Likewise, the one-to-one comparisons between the subtypes were made using GLM with each subtype being dummy coded as the reference subtype. However, this model was adjusted not only for the five covariates that were used but also for SuStaIn stage. In order to evaluate the clinical features throughout SuStaIn stage for each individual subtype, we calculated the correlation between each feature and SuStaIn stages using partial correlation analysis, after correcting for age, sex, education year, clinical diagnosis, and LEDD. We also evaluated, for each subtype and as a whole, the correlation between SuStaIn stage and each clinical feature. SuStaIn subtype

was also included as a covariate when the correlation was calculated as a whole.

To compare the difference of longitudinal clinical progression between subtypes, the linear mixed-effect model (LMEM) was applied after adjustment for age at baseline, sex, education year, SuStaIn stage at baseline, and LEDD. The clinical diagnosis was excluded from the adjustment since all subjects who underwent longitudinal clinical follow-up were patients with PSP. Disease duration was used as a time scale. A participant-specific random effect was incorporated because the intra-individual correlation was calculated for repeated measurements. All analyses were conducted in R environment (R Core Team, 2021; Vienna, Austria, https://www.R-project.org/). All hypothesis testing was two-tailed, with statistical significance defined as a p value < 0.05, unless otherwise indicated.

Role of funders

The Funders had no role in study design, data collection, data analyses, interpretation, or writing of report.

Results

Spatiotemporal patterns discovered by SuStaIn

We identified 2 subtypes of PSP using SuStaIn, each of which included 80 (subtype1, 57.1%) and 46 (subtype2, 32.9%) subjects, respectively, and 14 subjects (subtype0, 10%) were found in SuStaIn stage 0. For both subtypes, four distinctive ROI clusters were found that shared similar temporal patterns in positional variation diagram (Fig. 2a). The first ROI group involved subcortical regions, including RN, STN, Ra and GP (ROI-1). The second one involved other three subcortical regions, including SN, LC and PU (ROI-2). The third group involved one subcortical region (TH) and cerebellum (DE, CEWM) (ROI-3), and all cortical regions were considered as the last ROI group (ROI-4). The subtype1 showed the subsequent progression from subcortical regions to cortical regions where ROI-1 was first engaged, followed by ROI-2, ROI-3 and ROI-4. For subtype2, the progression started simultaneously in ROI-1, ROI-2 and ROI-4, and the progression in ROI-3 accompanied relatively later. In the early stages, subtype2 posed the synchronous progress in ROI-1 and ROI-2, whereas subtype1 presented the sequential progress from ROI-1 to ROI-2. Another characteristic temporal feature was the accumulation rate within ROIs. Although the subcortical-to-cortical spread was slower in subtype1 compared to that of subtype2, the spread-within-ROI was faster in the majority of ROIs in subtype1 once initiated (Fig. 2b). For instance, although the average 1-sigma onset position (red) of cortical regions for subtype1 was set later in SuStaIn stage compared to that for subtype2, the 3-sigma onset stage (magenta) was earlier for subtype1 than for subtype2 (Fig. 2a). The positional variation diagram corresponded well to the individual z-scores (Supplementary Figure S2), except for few outliers. Examples of cases with longitudinal PET follow-up of subtype1 and subtype2 were presented in Supplementary Figure S3.

Stability of subtype and stage

The CVIC was lowest when the number of subtypes for the model was two (Fig. 3a). The histogram of model log-likelihood indicated two distinctive clusters for two subtypes in both discovery and test dataset. However, the histogram resulted in a large overlap between two clusters in test dataset given three subtypes as an input (Fig. 3b). The positional variation diagram between discovery, cross-validation, and test dataset showed the distinctive three ROI groups, however, for subtype2, the accumulation in ROI-3 took place earlier especially in DE and CEWM in both cross-validation and test set compared to discovery set (Supplementary Figure S4).

Subtypes and clinical profiles

Table 1 summarizes the comparison regarding clinical features between subtypes. When compared to subtype0, both subtypes (subtype1, subtype2) were older (subtype1: $t = 2.23$, $p = 0.029$; subtype2: $t = 3.11$, $p = 0.003$; GLM) and had more patients with PSP (subtype1: $t = 9.72$, $p < 0.001$; subtype2: $t = 3.00$, $p = 0.004$; GLM), while no significant differences were found in terms of education year, sex, clinical phenotypes of PSP, LEDD and MMSE score. In particular, subtype1 showed overall more severe dysfunction than subtype0: total PSPrs ($t = 3.09$, $p = 0.003$; GLM), all stratified domains of PSPrs ($t = 2.56$–3.76, $p < 0.013$; GLM) except PSPrs-II, all four core clinical features of PSP suggested by MDS ($t = -2.24 \sim -5.26$, $p < 0.028$; GLM), MDS UPDRS-III ($t = 4.36$, $p < 0.001$; GLM), and H&Y scale ($t = 5.75$, $p < 0.001$; GLM). On the other hand, subtype2 presented severe degradation in PSPrs-IV ($t = 2.33$, $p = 0.024$; GLM) and two core clinical features of PSP suggested by MDS (O: $t = -3.63$, $p < 0.001$; A: $t = -2.58$, $p = 0.013$; GLM), compared to subtype0.

In the subtype1-to-subtype2 comparison, subtype2 was older ($t = 2.62$, $p = 0.010$; GLM) while other demographic profiles were similar. Subtype2 showed milder dysfunction in mentation (PSPrs-II; $t = -1.82$, $p = 0.072$; GLM), bulbar function (PSPrs-III: $t = -2.09$, $p = 0.039$; GLM), and limb motor function (PSPrs-V: $t = -2.05$, $p = 0.043$; GLM), compared to subtype1. Subtype 2 also presented lower disease severity scores in MDS UPDRS-III test ($t = -2.64$, $p = 0.010$; GLM), compared to subtype1.

Stages and clinical profiles

We evaluated the clinical features of each subtype with respect to the SuStaIn stages considering age, sex, education year, clinical diagnosis (HC/PSP), and LEDD as the confounders (Fig. 4, Supplementary Figure S5). For

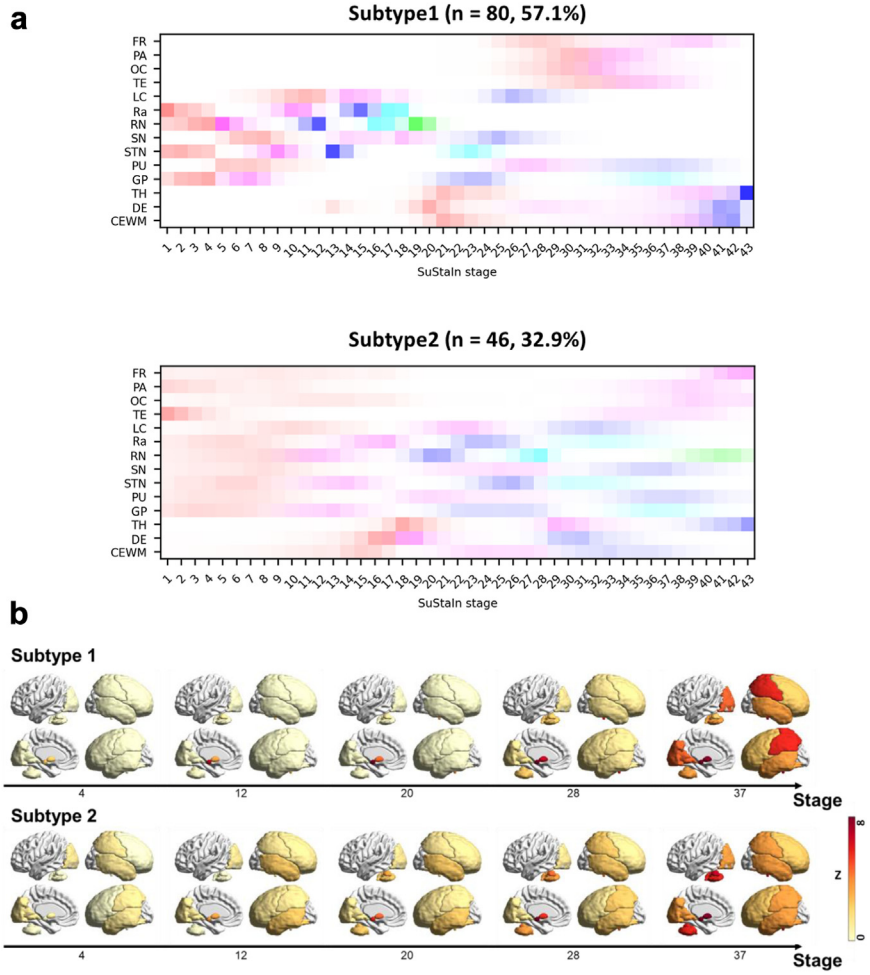

Fig. 2: **Subtype and Stage of PSP. a. Positional variation diagram estimated by SuStaIn**. The region of interest (ROI) includes frontal middle cortex (FR), parietal cortex (PA), occipital cortex (OC), temporal cortex (TE), locus coeruleus (LC), raphe nuclei (Ra), red nucleus (RN), substantia nigra (SN), subthalamic nucleus (STN), putamen (PU), globus pallidus (GP), thalamus (TH), dentate nucleus (DE), and cerebellum white matter (CEWM) for each subtype1 (top) and subtype2 (bottom). Red, magenta, blue, cyan, and green represent the z-score of 1,3,5,8, and 13 sigma along the stage for each ROI. **b. Average z-scores of each subtype along stage**.

subtype1, the MMSE score decreased, while total and all six stratified domains of PSPrs and MDS UPDRS-III increased along the SuStaIn stages. For subtype2, only PSPrs-VI and MDS UPDRS-III significantly increased with the SuStaIn stages. When considering both subtype1 and subtype2, the MMSE score decreased, while total PSPrs, all six domains of stratified PSPrs, MDS UPDRS-III and H&Y scale increased with the SuStaIn stages, except for PSPrs-IV that only showed a tendency ($p = 0.059$; partial correlation analysis).

Subtypes and clinical prognosis

Among the 43 patients with PSP who underwent longitudinal clinical follow-up, 1 was categorized as subtype0, 28 were subtype1, 14 were subtype2. The mean (standard deviation) follow-up year after baseline PET scan was 1.34 (0.46), 1.35 (0.53) for subtype1 and subtype2, respectively. Subtype2 was older ($t = 1.74$, $p = 0.090$; GLM) and had lower MDS-UPDRS III score ($t = -2.05$, $p = 0.049$; GLM) than subtype1 at baseline (Supplementary Table S2).

Although the sample size was limited, we preliminarily compared the clinical prognosis of PSP subtypes (Supplementary Table S4). After excluding confounders that included age at baseline, sex, education year, LEDD and SuStaIn stage at baseline, the LMEM analysis found that subtype2 was featured by a favorable prognosis in limb motor function (PSPrs-V), compared to subtype1. Albeit not significant, a slower trend of deterioration [annual difference ($\beta \pm SE$): -0.53 ± 0.26; $p = 0.061$; LMEM] was observed for the PSPrs-V in subtype2 than subtype1.

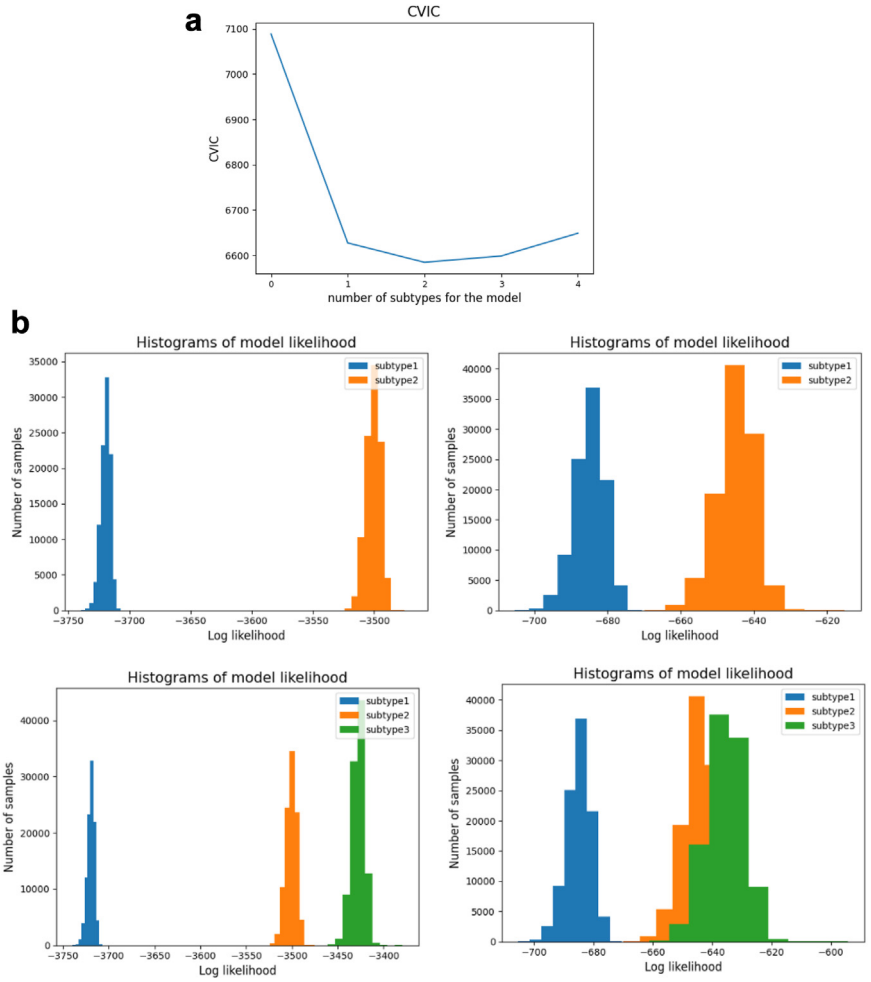

***Fig. 3:* SuStaIn and number of subtypes. a. Cross-validation information criteria (CVIC) and the number of subtypes. b. Histogram of model likelihood and the number of subtypes**. First row illustrates the histogram of likelihood when two subtypes were assumed for each discovery dataset (left) and test dataset (right). Second row depicts when three subtypes were considered.

Possible driven factor of distinct trajectories of tau deposition—findings from functional connectivity

Fig. 5 shows the group-wise FC difference between subtype1 and subtype2. Compared to subtype1, subtype2 mostly showed significant hypoconnectivity between pairs of ROIs. For example, the decreased FCs between TH and RN, CEWM and GP, FR and LC, and FR and DE was observed in subtype2 compared to those of subtype1. The only exception was the FCs between LC and RN, and LC and STN, where hyperconnectivity in subtype2 was discovered, compared to those in subtype1. Supplementary Figure S6 presents the comparison between subtype0 and subtype1, sbutype0 and subtype2.

Discussion

Utilizing the second-generation tau tracer [^{18}F]Florzolotau, which exhibits high affinity for both 3R- and 4R-tau, we identified two subtypes that displayed distinct stages of tau progression in PSP using a data-driven algorithm, SuStaIn. These subtypes were characterized by differences in age, dysfunction, and clinical severity was associated with the stages that were inferred by SuStaIn for both subtypes. Although limited in terms of sample size, the longitudinal data suggest that these varying spatiotemporal tau trajectories may reflect different clinical prognoses. Furthermore, we explored the potential mechanism of different tau transmission by analyzing the difference in FC between subtypes. Our current discoveries are anticipated to contribute to a comprehensive understanding of PSP, which may benefit various clinical, therapeutic, and epidemiological studies.

Recent findings have demonstrated that the heterogeneity of tau spreading patterns is rather common and systemic in Alzheimer's disease (AD), warranting a

reevaluation of the conventional binary notion (typical/atypical) of AD and a revisiting of tau pathological staging.[18,32,33] Likewise, it is critical to examine the heterogeneity of tau progress in PSP on the ground that PSP is the second most common tauopathy and the most common primary tauopathy. Furthermore, the diverse clinical presentations of patients with PSP[1,6] and the differences in cell-type specific vulnerability patterns among clinical phenotypes[8] indicate a potential heterogeneity in the pathological advancement of tau. However, the heterogeneity of the tau trajectories in PSP remains somewhat uncertain, attributing to two preceding findings. First, the regions that are involved in the initial engagement of tau are identical across the different clinical phenotypes of PSP, and this trend is observed in both *in vitro*[8] as well as *in vivo* studies.[15,16] Second, it is a widely accepted that most PSP-non-RS phenotypes will eventually develop features of PSP-RS.[6,7] SuStaIn partially accommodates both sides of heterogeneity hypotheses, as the model is fitted with z-scores linearly in ascending order that accounts for each subject. That is, the model uncovers the heterogeneity of the tau progress in PSP without excluding the scenario where all subtypes end up with tau engagement in the same ROIs. However, SuStaIn does not assume that the initial site of the tau progression is similar. In fact, one of the major differences between the two identified subtypes in this work was their early stage where one showed involvement in SN, PU, and cortical regions and the other did not. Different from the preceding studies, SuStaIn models the progression in two axes simultaneously: phenotypical and temporal. Therefore, the mismatch between the previous and current discoveries remains unclear. Prior studies did not consider both subtype and stage when modelling, therefore, may have conveyed the result from different stages across the subtypes being identical. In contrast, SuStaIn may have delivered modelling errors.

The proposed method adopted an unsupervised approach that does not require clinical diagnoses of data to find subtypes/stages of PSP, and the optimal number of subtypes suggested by the model was two: one with sequential involvement in subcortical and cortical ROIs (subtype1), and the other with relatively simultaneous involvement (subtype2). In subtype1, tau spread appeared first in the subcortical regions, then continued caudally (CEWM/DE), and in the end rostrally (FR, PA, OC, TE). In subtype2, tau accumulation proceeded simultaneously in the subcortical areas and other regions. The subjects who were assigned to either subtype with less than 75% of probability were mainly in the early SuStaIn stage. In fact, 76% of those were staged below 10 (Supplementary Figure S7). This suggests that it is challenging for SuStaIn to determine the subtype for the subjects who are in a very early stage of progression. When the model was fitted to one single subtype, the tau progression was similar as subtype1, which agrees well with the widely accepted notion (Supplementary Figure S8). However, the OC was the first cortical regions where tau accumulated throughout the disease course in this study (Fig. 2b) and the last cortical regions to face the first Z-score cutoff (Supplementary Table S3, Fig. 2a), which is partially different from the previous *in vitro* study that reconstructed topography of tau burden.[8] New tracers which possess a different ability to detect neuronal and astrocyte related tau may explain these mismatches in the future studies.[34] Otherwise, the spillover from the surrounding cerebellum may have caused the overestimation of the [^{18}F]Florzolotau signal in this area,[15] and the longitudinal imaging to track the tau propagation *in vivo* with the second-generation tau tracers may explain further together with the appropriate reference regions for semi-quantification. The tau progressions in the cortical regions need to be more carefully interpreted in this work as they are rather

	Subtype0	Subtype1	Subtype2
Number	14	80	46
Proportion female	0.64	0.41	0.54
Proportion PSP	0.21	0.99[a]	0.91[a,b]
Clinical subtypes (PSP-RS/PSP-non-RS)	1/2	42/37	27/15
Age (years)	55.9 (7.3)	64.4 (6.5)[a]	67.5 (7.3)[a,b]
Education (years)	11.2 (3.1)	10.0 (4.2)	9.8 (4.7)
MMSE	26.1 (4.4)	23.0 (6.0)	24.2 (4.8)
Disease duration (months)[c]	3.4 (6.7)	44.3 (30.0)[a]	45.4 (37.3)
PSPrs (total)[c]	6.2 (13.0)	29.8 (14.2)[a]	30.6 (18.0)
PSPrs-I[c]	1.4 (3.0)	6.2 (5.1)[a]	6.2 (5.1)
PSPrs-II[c]	0.9 (2.3)	3.1 (2.9)	3.1 (3.7)
PSPrs-III[c]	0.4 (0.7)	2.4 (1.8)[a]	2.0 (1.8)[b]
PSPrs-IV[c]	0.6 (1.9)	6.4 (3.5)[a]	6.2 (3.7)[a]
PSPrs-V[c]	1.1 (2.3)	4.6 (2.1)[a]	4.1 (2.5)[b]
PSPrs-VI[c]	1.9 (3.7)	8.3 (4.0)[a]	8.8 (5.1)
Ocular motor dysfunction (O1/O2/O3)[d]	0/1/0	42/26/0[a]	23/14/1[a]
Postural instability (P1/P2/P3)[d]	2/1/0	40/7/14[a]	23/6/5
Akinesia (A1/A2/A3)[d]	2/1/0	44/30/3[a]	19/22/0[a]
Cognitive dysfunction (C1/C2/C3)[d]	1/0/1	29/10/4[a]	12/7/1
MDS UPDRS-III[c]	10.0 (19.5)	41.8 (15.5)[a]	37.1 (20.5)[b]
H&Y[c]	0.7 (1.4)	3.3 (0.9)[a]	3.1 (1.3)
LEED (mg)[c]	21.4 (80.2)	417.2 (301.1)	425.2 (341.9)

Data are expressed as means (standard deviations) unless otherwise indicated. A generalized linear model (GLM) was fitted for the comparison of means of different variables between subtypes in the discovery sample after correction for age (except in the case of age), sex (except in the case of sex), education (except in the case of education), clinical diagnosis (that is, HC, PSP; except in the case of clinical diagnosis), LEED (except in the case of LEED) and SuStaIn stage (except comparisons with S0). Abbreviations: PSP, progressive supranuclear palsy; MMSE, Mini-Mental State Examination; PSPrs, progressive supranuclear palsy rating scale; MDS UPDRS-III, part III of Movement Disorder Society Sponsored Revision of the Unified Parkinson's Disease Rating Scale; H&Y, Hoehn and Yahr scale; LEDD, L-dopa equivalent daily dose; PSP-RS, progressive supranuclear palsy-Richardson's syndrome; PSP-non-RS, other PSP subtypes expect progressive supranuclear palsy-Richardson's syndrome. All *p* values were not corrected for multiple comparisons. [a]$p < 0.05$ (versus subtype0). [b]$p < 0.05$ (versus subtype1). [c]Healthy controls were assigned a score of 0 for these items. [d]Levels with lower numbers are considered to contribute higher certainty to a diagnosis of PSP than levels with higher numbers. Those with normal function in the specific domains are coded as 4 for the analysis.

Table 1: **The comparison between subtypes in the discovery set.**

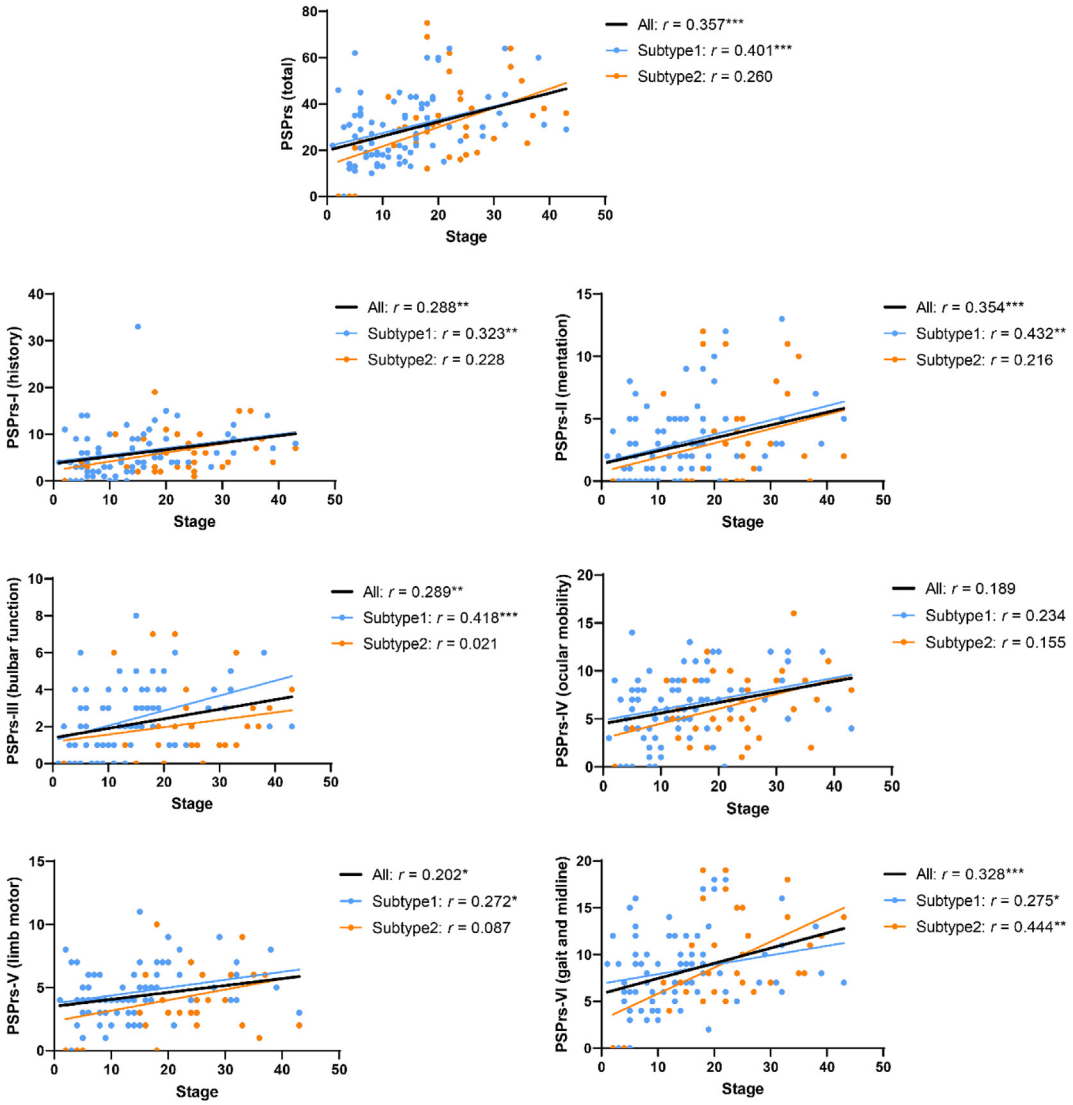

Fig. 4: **Partial correlations between SuStaIn stages and PSPrs scores**. The correlation coefficient (r) and p values are noted after correcting for age, sex, education year, clinical diagnosis (healthy control/progressive supranuclear palsy), and L-dopa equivalent daily dose. When analyzing the combination of subtype1 and subtype2, SuStaIn subtype was also included as a covariate. *$p < 0.05$, **$p < 0.01$, ***$p < 0.001$. Abbreviation: PSPrs, progressive supranuclear palsy rating scale.

estimated in macroscale. For instance, the dorsolateral prefrontal cortex (DLPFC) is the region which largely relates to the clinical features in patients, however, was integrated as FR in this study. Regardless, the tau spreading pattern was consistent between the discovery set, cross-validation set, and test set in subtype1 but not in subtype2 possibly due to the small sample size (Supplementary Figure S4).

Different pathological trajectories may represent subtle variations in clinical presentations, potential differences in prognosis and therapeutic reaction. The identified subtype1 was characterized as a younger age and a higher disease severity in mentation, bulbar function, limb motor. Meanwhile, the differences found in comparison of subtype1/2 to subtype0 were similar to those between HC group and PSP group, which might result from the fact that the majority of subtype0 was HCs (11/14, 79%). Further validation in larger, demographically comparable cohorts of controls and PSP patients is required. As pathological change is strongly associated with disease severity, *in vivo* tau biomarkers are capable of tracking progression, hence, may serve as sensitive indices for the therapeutic assessment.

Staging system based on pathological evidence plays an essential role in quantification of neurodegenerative disorders,[35,36] however, there is little consensus on how

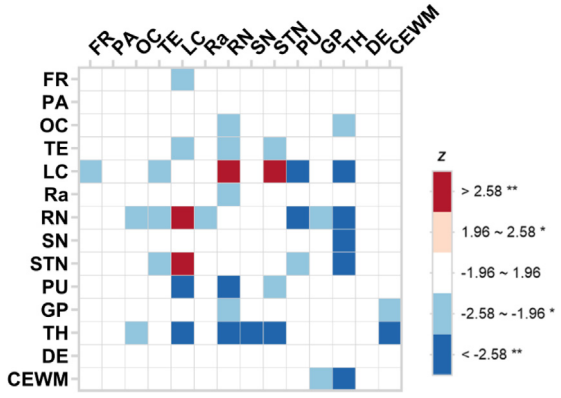

***Fig. 5:* Group-wise seed-based functional connectivity difference between subtype1 and subtype2**. Using subtype1 as the reference group, the negative and positive Z scores represent decreased and increased functional connectivity, respectively, in subtype2 after the correction for age, sex, education year, clinical diagnosis (HC/PSP), LEDD, and SuStaIn stage. *$p < 0.05$, **$p < 0.01$. Abbreviation: FR, frontal cortex; PA, parietal cortex; OC, occipital cortex; TE, temporal cortex; LC, locus coeruleus; Ra, raphe nuclei; RN, red nucleus; SN, substantia nigra; STN, subthalamic nucleus; PU, putamen; GP, globus pallidus; TH, thalamus; DE, dentate nucleus; CEWM, cerebellum white matter.

to quantify tau burden in PSP. Although conventional semi-quantification (i.e., SUVr) in disease-specific ROIs showed significant correlations with clinical assessments,[12] tau burden in these methods is rather measured in the specific regions, separately or as a whole, which do not account for tau propagation throughout disease course that moves from region to region. The applied method avoids this limitation by adopting a mixture linearized modeling that considers the tau accumulation in multi-region.[8] Therefore, the SuStaIn stages may serve as a quantification method, more accurately, which calibrates the tau burden in each subtype. It's worth noting that associations between the SuStaIn stage and the clinical severity were less significant in subtype2 than subtype1 in most clinical variables, which might result from the relatively discordant trajectories of tau deposition in subtype2. Although we identified two subtypes in this study, it is highly possible that subtype2 is further subdivided into several subtypes with more vPSP data (Supplementary Figure S9).

Despite the limited cases with longitudinal clinical follow-up, our preliminary result suggested a better prognosis in subtype2 than subtype1. Different clinical prognoses in vPSP have also been studied. Jabbari and colleagues reported that PSP-cortical variants together with PSP-RS had worse prognosis than PSP-subcortical variants.[37] Street and colleagues found that PSP-RS had worse prognosis than PSP-non-RS combining both PSP-cortical and PSP-subcortical variants.[38] Given that the current study could only explore the relationship between SuStaIn subtypes and clinical variants (PSP-RS/PSP-non-RS) roughly due to the limited and unbalanced sample size of each phenotype in the PSP-non-RS group, the connection between these two subtypes remains to be investigated. Furthermore, it is evident that the SuStaIn model would benefit from an increased sample size in the early stages, namely HC. In parallel, the binding pattern in brainstem and deep cerebellar structures within HC should be studied. Collectively, the current finding confirms and expands the potential value of tau PET imaging in predicting the clinical progression in the patients with PSP. Further exploration will be made to validate and extend the current preliminary observations with a larger number of participants from the ongoing PSPNI both cross-sectionally and longitudinally.

Neuronal connectivity is agreed as a pivotal channel for tau spreading in tauopathies.[39] Different hypotheses lead to different predictions about the relationship between tau burden and connectivity; while the trans-neuronal spread hypothesis predicts that regions that are more strongly interconnected would accrue more tau pathology, the trophic support hypothesis conversely forecasts a negative relationship between tau burden and clustering coefficient. To explain the possible underlying mechanism for the distinct spatiotemporal trajectories, the difference in the regional-level FC between-subtype was investigated. Hypoconnectivity was observed in subtype2 compared to subtype1, which was consistent with previous [^{18}F]flortaucipir PET study that unlike AD in which tau spread in a prion-like manner, the pathological tau accumulation in PSP was selectively vulnerable due to the increased metabolic demand and a lack of trophic support.[40] Besides, both increased and decreased FC network alterations have been reported in PSP previously, and the former is considered to be a temporally adaptive change that may precede the latter.[21] In the current study, the relatively increased FC in subtype2 than subtype1 was seen as well. Longitudinal follow-ups are required to answer whether this was the compensatory mechanisms which would disintegrate with disease progression.[21] It is worth noting that the assessment of functional connectivity was conducted without taking into account possible adaptations that might occur across varying stages of the disease.

We acknowledge limitations of the present study. First, the single-center and single-tracer design with relatively limited sample size requires the external validity of the results. While some clinical subtypes such as PSP with predominant speech/language disorder (PSP-SL) (i.e., 2% in the National Health Service specialist PSP clinic in Cambridge, UK[38]) are quite rare within the disease spectrum, future study covering the entire clinical phenotypes and maintaining a distribution consistent with epidemiological data is necessary. Notably, vPSP represents a significantly diverse group. By enhancing the model with multiple tau tracers, we

can further unravel the complex nature of PSP. Second, [^{18}F]Flortaucipir is a tau tracer, and its findings may have captured signals from other tauopathies like corticobasal degeneration (CBD), AD, or primary age-related tauopathy (PART). To minimize this potential confounding effect, we strictly adhered to MDS criteria for PSP and excluded PSP-CBS while modeling the subtypes. However, it is important to acknowledge that a definitive diagnosis can only be confirmed postmortem, and there remains a slight possibility of a mixing effect in this study. Third, the stability and progression of PSP subtypes over time have not been investigated due to the lack of adequate longitudinal tau PET imaging. Longitudinal clinical follow-up sample size and duration are limited by the fact that the PSPNI is a nascent clinical cohort. Fourth, the reference region for deriving SUVr in second generation tau PET is an area that has not been extensively explored in the current literatures, although cerebellum is mostly used.[15,16] In our study, we opted to use cerebellar gray matter as a reference region to minimize the inclusion of tau signal. To achieve this, we specifically excluded the dentate and white matter regions within the cerebellum in this work. However, as SuStaIn primarily relies on SUVr values for modeling, investigating this aspect warrants a separate study. Fifth, only one aspect of the possible underlying mechanisms has been investigated and others such as metabolic connectivity remain to be explored.[41] Finally, this study did not confirm the existence of amyloid pathologies through methods such as cerebrospinal fluid analysis or PET scans. The lack of such verification may hint at the simultaneous spread of tau proteins, which is a key characteristic of the initial stages of AD pathology.

Contributors

All authors read and approved the final version of the manuscript.

Study concept and design: Chuantao Zuo, Kuangyu Shi, Jian Wang.

Data acquisition: the PSPNI.

Analysis, or interpretation of data: Jimin Hong, Jiaying Lu, Fengtao Liu, Min Wang, Xinyi Li, Leonor Lopes, Christoph Clement, Yihui Guan, Mei Tian.

Verifying the underlying data: Min Wang, Xinyi Li.

Drafting of the manuscript: Jimin Hong, Jiaying Lu.

Critical revision of the manuscript for important intellectual content: Fengtao Liu, Chuantao Zuo, Kuangyu Shi, Jian Wang, Tzu-Chen Yen, Axel Rominger, Matthias Brendel.

Data sharing statement

Fully anonymized data will be shared by request from qualified investigators (Chuantao Zuo), subject to approval by the China Human Genetic Resources Administration Office. Data transfer will have to comply with the Regulations of the People's Republic of China. The machine-learning algorithm, SuStaIn (Subtype and Stage Inference) used for the preparation for this article can be found at: https://github.com/ucl-pond/pySuStaIn.

Declaration of interests

Kuangyu Shi receives support from Novartis, Siemens Healthineers, Hermes Medical Solution, DosiSoft, Varian, THQ Medical Products, QDose, PMOD, Boston Scientific, SIRTEX, MIM Software, and the ICPO Foundation. Matthias Brendel is a member of the Neuroimaging Committee of the EANM and the SNMMI Brain Imaging Council. Matthias Brendel received speaker honoraria from Roche, GE healthcare and Life Molecular Imaging and is an advisor of Life Molecular Imaging. Axel Rominger receives support from Novartis and Siemens Healthineers. Tzu-Chen Yen is an employee of APRINOIA Therapeutics Co., Ltd (Suzhou, China). All other authors have no conflicts of interest to declare.

Acknowledgements

We would like to express our sincere appreciation to the study participants and their relatives. We are grateful to APRINOIA Therapeutics for the provision of the [^{18}F]Florzolotau precursor. This work was supported by grants from the National Natural Science Foundation of China (82272039, 81971641, 82021002, 92249302, 82171252 and 81701250); Swiss National Science Foundation (188350); the STI2030-Major Project of China (2022ZD0211600); the Clinical Research Plan of Shanghai Hospital Development Center of China (SHDC2020CR1038B); and the National Key R&D Program of China (2022YFC2009902, 2022YFC2009900), the China Scholarship Council (202006100181); the Deutsche Forschungsgemeinschaft (DFG) under Germany's Excellence Strategy within the framework of the Munich Cluster for Systems Neurology (EXC 2145 SyNergy, ID 390857198), the Jacques and Gloria Gossweiler Foundation.

Appendix A. Supplementary data

Supplementary data related to this article can be found at https://doi.org/10.1016/j.ebiom.2023.104835.

References

1 Höglinger GU, Respondek G, Stamelou M, et al. Clinical diagnosis of progressive supranuclear palsy: the movement disorder society criteria. *Mov Disord*. 2017;32:853–864.
2 Dugger BN, Hentz JG, Adler CH, et al. Clinicopathological outcomes of prospectively followed normal elderly brain bank volunteers. *J Neuropathol Exp Neurol*. 2014;73:244–252.
3 Nogami A, Yamazaki M, Saito Y, et al. Early stage of progressive supranuclear palsy: a neuropathological study of 324 consecutive autopsy cases. *J Nippon Med Sch*. 2015;82:266–273.
4 Yoshida K, Hata Y, Kinoshita K, et al. Incipient progressive supranuclear palsy is more common than expected and may comprise clinicopathological subtypes: a forensic autopsy series. *Acta Neuropathol*. 2017;133:809–823.
5 Dickson DW, Ahmed Z, Algom AA, et al. Neuropathology of variants of progressive supranuclear palsy. *Curr Opin Neurol*. 2010;23:394–400.
6 Respondek G, Stamelou M, Kurz C, et al. The phenotypic spectrum of progressive supranuclear palsy: a retrospective multicenter study of 100 definite cases. *Mov Disord*. 2014;29:1758–1766.
7 Boxer AL, Yu JT, Golbe LI, et al. Advances in progressive supranuclear palsy: new diagnostic criteria, biomarkers, and therapeutic approaches. *Lancet Neurol*. 2017;16:552–563.
8 Kovacs GG, Lukic MJ, Irwin DJ, et al. Distribution patterns of tau pathology in progressive supranuclear palsy. *Acta Neuropathol*. 2020;140:99–119.
9 Williams DR, Holton JL, Strand C, et al. Pathological tau burden and distribution distinguishes progressive supranuclear palsy-parkinsonism from Richardson's syndrome. *Brain*. 2007;130:1566–1576.
10 Briggs M, Allinson KSJ, Malpetti M, et al. Validation of the new pathology staging system for progressive supranuclear palsy. *Acta Neuropathol*. 2021;141:787–789.
11 Tagai K, Ono M, Kubota M, et al. High-contrast in vivo imaging of tau pathologies in alzheimer's and non-alzheimer's disease tauopathies. *Neuron*. 2021;109:42–58.e8.
12 Li L, Liu FT, Li M, et al. Clinical utility of 18F-APN-1607 tau PET imaging in patients with progressive supranuclear palsy. *Mov Disord*. 2021;36:2314–2323.
13 Malpetti M, Kaalund SS, Tsvetanov KA, et al. In vivo 18 F-flortaucipir PET does not accurately support the staging of progressive supranuclear palsy. *J Nucl Med*. 2022;63:1052–1057.
14 Soleimani-Meigooni DN, Iaccarino L, La Joie R, et al. 18F-flortaucipir PET to autopsy comparisons in Alzheimer's disease and other neurodegenerative diseases. *Brain*. 2020;143:3477–3494.

15 Liu F-T, Lu J-Y, Li X-Y, et al. 18F-Florzolotau PET imaging captures the distribution patterns and regional vulnerability of tau pathology in progressive supranuclear palsy. *Eur J Nucl Med Mol Imaging*. 2023;50(5):1395–1405.
16 Brendel M, Barthel H, Van Eimeren T, et al. Assessment of 18F-PI-2620 as a biomarker in progressive supranuclear palsy. *JAMA Neurol*. 2020;77:1408–1419.
17 Young AL, Marinescu RV, Oxtoby NP, et al. Uncovering the heterogeneity and temporal complexity of neurodegenerative diseases with Subtype and Stage Inference. *Nat Commun*. 2018;9:4273.
18 Vogel JW, Young AL, Oxtoby NP, et al. Four distinct trajectories of tau deposition identified in Alzheimer's disease. *Nat Med*. 2021;27:871–881.
19 Aksman LM, Wijeratne PA, Oxtoby NP, et al. pySuStaIn: a Python implementation of the Subtype and Stage Inference algorithm. *SoftwareX*. 2021;16:100811.
20 Collij LE, Salvadó G, Wottschel V, et al. Spatial-temporal patterns of β-amyloid accumulation: a subtype and stage inference model analysis. *Neurology*. 2022;98:e1692–e1703.
21 Rosskopf J, Gorges M, Müller HP, et al. Intrinsic functional connectivity alterations in progressive supranuclear palsy: differential effects in frontal cortex, motor, and midbrain networks. *Mov Disord*. 2017;32:1006–1015.
22 Franzmeier N, Brendel M, Beyer L, et al. Tau deposition patterns are associated with functional connectivity in primary tauopathies. *Nat Commun*. 2022;13:1362.
23 Liu FT, Li XY, Lu JY, et al. 18F-Florzolotau tau positron emission tomography imaging in patients with multiple system atrophy–parkinsonian subtype. *Mov Disord*. 2022;37:1915–1923.
24 Golbe LI, Ohman-Strickland PA. A clinical rating scale for progressive supranuclear palsy. *Brain*. 2007;130:1552–1565.
25 Goetz CG, Tilley BC, Shaftman SR, et al. Movement disorder society-sponsored revision of the unified Parkinson's disease rating scale (MDS-UPDRS): scale presentation and clinimetric testing results. *Mov Disord*. 2008;23:2129–2170.
26 Zhu S, Ju Z, Wu P, et al. The Parkinson's disease progression neuroimaging initiative. *Behav Neurol*. 2021;2021:1–8.
27 Ju Z, Li Z, Lu J, et al. In vivo tau burden is associated with abnormal brain functional connectivity in alzheimer's disease: a [18F]-Florzolotau study. *Brain Sci*. 2022;12:1355.
28 Fonteijn HM, Modat M, Clarkson MJ, et al. An event-based model for disease progression and its application in familial Alzheimer's disease and Huntington's disease. *Neuroimage*. 2012;60:1880–1889.
29 Young AL, Oxtoby NP, Daga P, et al. A data-driven model of biomarker changes in sporadic Alzheimer's disease. *Brain*. 2014;137:2564–2577.
30 Archetti D, Young AL, Oxtoby NP, et al. Inter-cohort validation of sustain model for alzheimer's disease. *Front Big Data*. 2021;4:1–13.
31 Xia M, Wang J, He Y. BrainNet Viewer: a network visualization tool for human brain connectomics. *PLoS One*. 2013;8:e68910.
32 Hong J, Kang SK, Alberts I, et al. Image-level trajectory inference of tau pathology using variational autoencoder for Flortaucipir PET. *Eur J Nucl Med Mol Imaging*. 2022;49:3061–3072.
33 Young CB, Winer JR, Younes K, et al. Divergent cortical tau positron emission tomography patterns among patients with preclinical alzheimer disease. *JAMA Neurol*. 2022;79:592–603.
34 Ballweg A, Klaus C, Vogler L, et al. [^{18}F]F-DED PET imaging of reactive astrogliosis in neurodegenerative diseases: preclinical proof of concept and first-in-human data. *J Neuroinflammation*. 2023;20:68.
35 Braak H, Braak E. Neuropathological stageing of Alzheimer-related changes. *Acta Neuropathol*. 1991;82:239–259.
36 Jecmenica Lukic M, Kurz C, Respondek G, et al. Copathology in progressive supranuclear palsy: does it matter? *Mov Disord*. 2020;35:984–993.
37 Jabbari E, Holland N, Chelban V, et al. Diagnosis across the spectrum of progressive supranuclear palsy and corticobasal syndrome. *JAMA Neurol*. 2020;77:377–387.
38 Street D, Malpetti M, Rittman T, et al. Clinical progression of progressive supranuclear palsy: impact of trials bias and phenotype variants. *Brain Commun*. 2021;3:fcab206.
39 Gibbons GS, Lee VMY, Trojanowski JQ. Mechanisms of cell-to-cell transmission of pathological tau: a review. *JAMA Neurol*. 2019;76:101–108.
40 Cope TE, Rittman T, Borchert RJ, et al. Tau burden and the functional connectome in Alzheimer's disease and progressive supranuclear palsy. *Brain*. 2018;141:550–567.
41 Wang M, Schutte M, Grimmer T, et al. Reducing instability of inter-subject covariance of FDG uptake networks using structure-weighted sparse estimation approach. *Eur J Nucl Med Mol Imaging*. 2022;50:80–89.